Received: 16 March 2017 | Revised: 14 January 2018 | Accepted: 1 February 2018

DOI: 10.1002/qj.3261

RESEARCH ARTICLE

Quarterly Journal of the Royal Meteorological Society RMetS

The effect of potential vorticity fluxes on the circulation of the tropical upper troposphere

Sebastián Ortega | Peter J. Webster | Violeta Toma | Hai-Ru Chang

College of Sciences, School of Earth and Atmospheric Sciences, Georgia Institute of Technology, Atlanta, Georgia

Correspondence
Peter J. Webster, College of Sciences, School of Earth and Atmospheric Sciences, Georgia Institute of Technology, Atlanta, GA 30332.
Email: pjw@eas.gatech.edu

Funding information
Climate Dynamics Division of the National Science Foundation, NSF-AGS 1638256, NSF-AGS 0965610.

With simple analytical arguments, we suggest that the subtropical westerly jets, the equatorial easterly winds, the westerly ducts (i.e. regions of westerly winds over the Equator), and the tropical upper tropospheric troughs, are coupled via potential vorticity (PV) dynamics. We suggest that deep tropical convection leads to advective PV fluxes towards the Poles over the subtropical westerly jets, triggering Rossby waves on the jet, and leading to advective PV fluxes towards the Equator when the Rossby waves break over the westerly ducts. Moreover, we show that the advective PV fluxes towards the Poles closely balance those towards the Equator, and suggest that this close balance is to be expected from the impermeability theorem. We then argue that small imbalances of these advective PV fluxes play an important role in maintaining the upper tropospheric mean flow of the tropical atmosphere.
We test our ideas using a shallow-water model of the atmosphere, where diabatic heating terms are absent, and show how imbalances in the advective PV fluxes of a shallow-water model maintain its mean flow. We focus on the periodicity of the shallow-water models to study the effect of transient eddies and relate our results to previous studies.

KEYWORDS
impermeability theorem, large-scale tropical circulation, potential vorticity, Rossby wave breaking, tropical upper tropospheric trough, tropical zonal momentum balance, westerly ducts

1 | INTRODUCTION

Three major features dominate the climatology of the tropical upper troposphere: westerly jet streams, upper tropospheric easterly winds, and westerly ducts. The jet streams are the well-known bands of strong westerly winds that lie over the Subtropics. The upper tropospheric easterly winds are regions of enhanced easterly winds, in between these westerly jet streams, that extend around most of the Tropics (Lee, 1999; Dima *et al.,* 2005). The westerly ducts (Webster and Holton, 1982; Tomas and Webster, 1994) are regions of westerly winds that separate or intrude into the upper tropospheric easterly winds (Figure 1a,b).

In the broader literature, the term "westerly ducts" is used to refer exclusively to the westerly winds present over the equatorial Pacific and Atlantic Oceans during boreal winter (Webster and Holton, 1982). Here, though, we will use the term to refer to the westerly winds that are present over, or that intrude into, the equatorial upper troposphere throughout the year. That is, we will not make a distinction between the westerly ducts, present during boreal winter, and the tropical upper tropospheric trough (TUTT: Gray, 1968; Sadler,

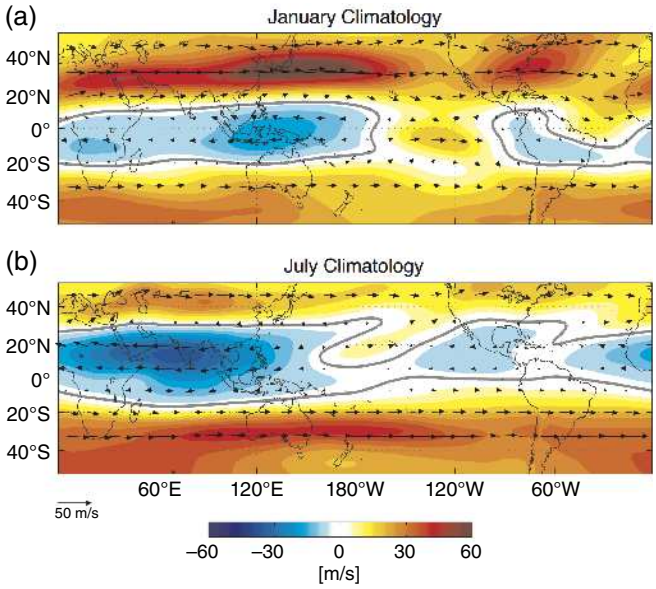

FIGURE 1 (a) January and (b) July climatological winds (black arrows) and zonal wind speed (colour shading) on the 370 K isentrope. ERA-Interim data [Colour figure can be viewed at wileyonlinelibrary.com]

1976), present during the boreal summer over the North Pacific and Atlantic Oceans. Thus, we will refer to the TUTT as the boreal summer manifestation of the westerly ducts. As will become evident, this distinction is justified as similar dynamics are involved in the formation of both the westerly ducts and the TUTT.

The westerly jet streams, the upper tropospheric easterly winds and the westerly ducts all display a strong annual cycle but remain identifiable, in different forms and locations, throughout the year. Consider the Northern Hemisphere for an example. During January, the Northern Hemisphere's westerly jet stream is strong and closest to the Equator (e.g. Dima *et al.,* 2005), the westerly ducts are strong and over the Equator, and the longitudinal extent of the easterly winds is interrupted by the westerly ducts. During July, the Northern Hemisphere's westerly jet stream is weak and displaced towards the north, the westerly ducts sit northwest relative to their position in January (and are known at this time as TUTTs), and the easterlies more or less extend around the Equator. Over South Asia, the northward displacement of the subtropical westerly jet and the intensification of the equatorial easterly winds, known then as the easterly jet (Koteswaram, 1958), reflect the formation of the upper tropospheric monsoon anticyclone (e.g. Wu *et al.,* 2014) as described by Ortega *et al.* (2017) and as is evident in Figure 1b. A similar, although weaker, transition occurs over North America.

The distinction between these upper tropospheric circulation features is useful as it correlates with the occurrence of different dynamical processes. For example, within the westerly jet streams Rossby waves constantly propagate eastward (e.g. Sardeshmukh and Hoskins, 1988; Chang and Yu, 1999). Within the westerly ducts these Rossby waves move equatorward and break[1] (Kiladis and Weickmann, 1992; Tomas and Webster, 1994; Slingo, 1998; Postel and Hitchman, 1999; Waugh and Polvani, 2000; Knippertz, 2007; Ortega *et al.,* 2017). And within the equatorial easterly winds, upper tropospheric eddies, formed as by-products of the Rossby wave-breakings, are transported westward near the Equator and slowly northward back towards the subtropical westerly jet (Koteswaram and George, 1958; Slingo, 1998; Ortega *et al.,* 2017). Moreover, as noted by Dima *et al.* (2005), the upper tropospheric circulation features also correlate with the stationary dynamical features of the upper troposphere, with easterly winds occurring to the west of the stationary Rossby wave couplet that results from seasonal convection (as in Gill, 1980, and Webster, 1972), and westerly ducts occurring to the east of this couplet, within the stationary Kelvin wave response to the seasonal convection.

In this article, we study how these circulation features are coupled and how they are maintained via potential vorticity (PV) dynamics. We suggest that deep tropical convection leads to advective PV fluxes that are poleward over the subtropical westerly jets and that these fluxes are nearly balanced by advective PV fluxes that are equatorward over the westerly ducts. We also suggest that imbalances between these poleward and equatorward advective PV fluxes are needed in order to maintain the subtropical westerly jets, the equatorial easterlies and the westerly ducts.

In section 2 we review the data, the methods and the concepts that will be used in this study. In section 3 we revisit the large-scale circulation features of the upper troposphere as seen through its PV field. In section 4, we present an analytical argument suggesting that advective PV fluxes on the tropical upper troposphere are a response to equatorial convection and Rossby wave breaking, and that imbalances in these fluxes help maintain the upper tropospheric circulation. In section 5, we explore these ideas for two different simulations of a shallow-water model. Our results are summarized in section 6.

2 | DATA AND METHODS

To study the large-scale circulation of the tropical upper troposphere, we use ERA-Interim reanalysis data (Dee *et al.,* 2011) on isentropic surfaces from the year 1980 to 2013. Specifically, we use daily averages of the absolute vorticity and wind fields on the 370 K isentrope to compute climatological PV fluxes on the tropical upper troposphere.

We then use a shallow-water model as a prototype to gain insight into the effect that upper tropospheric PV fluxes might have on the circulation of the tropical upper troposphere. The

[1]The breaking of these Rossby waves is understood in the sense discussed in McIntyre and Palmer (1983). A Rossby wave is said to break when potential vorticity contours, which sustain the wave, are irreversibly deformed, leading to the mixing of the potential vorticity field instead of the propagation of the Rossby wave.

model, described in Arakawa and Lamb (1981), seeks the solution of the momentum and mass conservation equations on an equatorial beta plane[2] resulting from an external forcing (S). The governing equations of this model are

$$\frac{\partial \boldsymbol{v}}{\partial t} - q h \boldsymbol{k} \times \boldsymbol{v} = -\nabla [K_E + g h] - k \boldsymbol{v}, \quad (1)$$

$$\frac{\partial h}{\partial t} + \nabla \cdot (h \boldsymbol{v}) = S, \quad (2)$$

where $\boldsymbol{v}$ is the wind vector, $\boldsymbol{k}$ a unit vector pointing upwards, $q = \eta/h$ is the potential vorticity of the flow, η the absolute vorticity, h the depth of the shallow water model, $K_E = |\boldsymbol{v}|^2/2$ the kinetic energy of the flow, g the acceleration due to gravity, k a linear damping term, and S a mass source–sink term which is analogous to a heating sink–source.

We define S as a relaxation towards an equilibrium height h_e, within a time-scale τ, as in Hsu and Plumb (2000):

$$S = \frac{(h - h_e)}{\tau}. \quad (3)$$

This definition is intended to represent the divergent flow set by convection in the upper troposphere. We define the equilibrium height (h_e) following Webster and Chang (1988):

$$h_e = H + A \exp\left\{ -\left|\frac{\lambda - \lambda_0}{\sigma_\lambda}\right| - \left(\frac{\phi - \phi_0}{\sigma_\phi}\right)^2 \right\}, \quad (4)$$

where H is a reference height, A is the amplitude of the perturbation to H represented by the second term on the right-hand side, λ_o and ϕ_o determine the location of the perturbation, and σ_λ and σ_ϕ the longitudinal and latitudinal scale of the perturbation.

For all experiments conducted, we initialize the shallow-water model from a state of rest relative to the surface. We then turn on the forcing (i.e. S) and allow the model to evolve until either a steady or a periodic state is reached. We consider that a steady state has been reached when $a(x, y, t) = a(x, y, t + t')$ for all fields "a" and for any t'. We consider that a periodic state has been reached when, for a given period T, $a(x, y, t) \cong a(x, y, t + T)$.

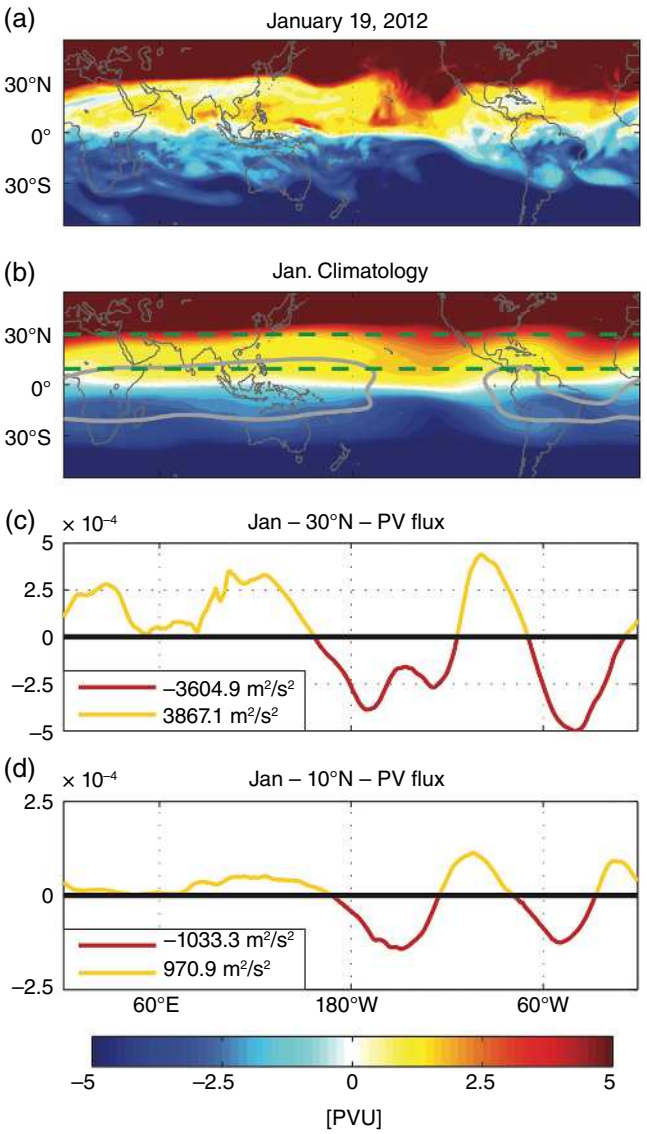

FIGURE 2 (a) 370 K PV field (PV units) during 19 January 2012. (b) Climatological 370 K PV field for January (colour shading), boundary between westerlies and easterlies (grey contour), and lines over which PV fluxes are computed (green dashed lines). (c) PV fluxes along 30°N (red and yellow curve) and the integrated negative and positive fluxes along 30°N (legend). (d) PV fluxes along 10°N and the integrated negative and positive fluxes along 10°N. ERA-Interim data [Colour figure can be viewed at wileyonlinelibrary.com]

3 | PV VARIABILITY ON THE 370 K ISENTROPE

The three upper tropospheric circulation features described in section 1 can also be identified in the upper tropospheric PV field displayed in Figures 2 and 3. The westerly jets are identified with sharp meridional gradients of PV in the Subtropics (McIntyre, 2008). The westerly ducts occur as large-scale PV troughs that extend towards the Equator. And the equatorial easterly winds appear as regions of relatively low PV to the west of the midlatitude PV troughs (Figures 2a,b and 3a,b: Hoerling, 1992).

Moreover, the different dynamical processes that are associated with each feature are apparent in movies of the PV fields (see the supplementary movie of Ortega *et al.* (2017), and the American Geophysical Union Bjerknes Lecture of Hoskins (2014)). The propagation of Rossby waves in the subtropical westerly jet appears as a series of propagating synoptic-scale PV troughs and ridges over the midlatitudes along the jet (e.g. Chang and Yu, 1999). Rossby wave breaking, which occurs when the PV troughs and ridges propagate over and to the west of the westerly duct, appears as a stretching, thinning and tilting of the synoptic PV troughs as they lose their coherence (e.g. Scott *et al.*, 2001; Scott and

[2]We also used the National Center for Atmospheric Research (NCAR)'s shallow-water model (Hack and Jakob, 1992) to corroborate our results. The model is available online at http://www.csm.ornl.gov/chammp/stswm/.

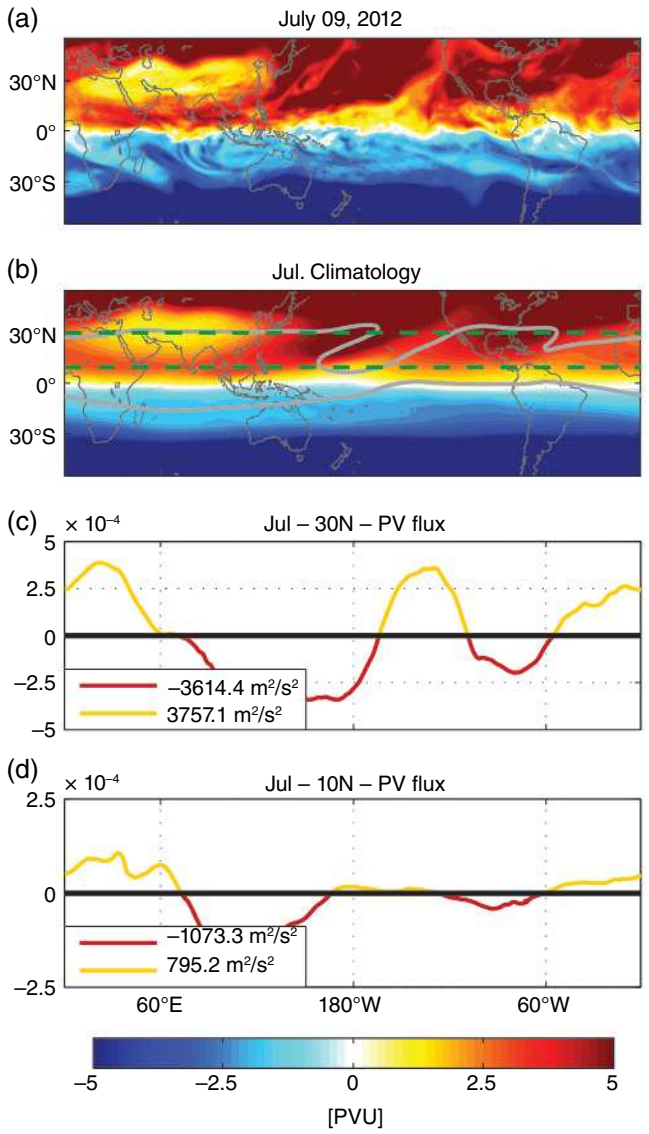

FIGURE 3 (a) 370 K PV field (PV units) during 9 July 2012. (b) Climatological 370 K PV field for July (colour shading), boundary between westerlies and easterlies (grey contour), and lines over which PV fluxes are computed (green dashed lines). (c) PV fluxes along 30°N (red and yellow curve) and the integrated negative and positive fluxes along 30°N (legend). (d) PV fluxes along 10°N and the integrated negative and positive fluxes along 10°N. ERA-Interim data [Colour figure can be viewed at wileyonlinelibrary.com]

Cammas, 2002; Garny and Randel, 2013; Ortega *et al.,* 2017). The advection of eddies over the equatorial easterly winds appears as upper tropospheric PV filaments and eddies, a by-product of the breaking of the synoptic PV troughs, that are advected westward and slowly northward back toward the midlatitudes (e.g. Slingo, 1998; Liu *et al.,* 2007; Plumb, 2007).

Figures 2a and 3a suggest that the upper tropospheric features behave in the manner just described. The figures show the upper tropospheric PV field over Asia and the Pacific Ocean for a representative day during January and July of 2012. They show examples of Rossby waves breaking over, or to the west of the westerly ducts (as discussed in Waugh and Polvani, 2000).

During the day in January (Figure 2a), the PV field over Asia was mostly zonal, and two PV troughs were present over the North Pacific Ocean: the first just east of Japan and the second just west of North America over the Pacific Ocean westerly duct. The second PV trough stretched much deeper into the Equator than the first, and had some of its PV scattered to its west over the region of equatorial easterly winds.

During the day in July (Figure 3a), the PV field had a small trough over central Asia and a large trough over the Pacific Ocean. The PV trough over the Pacific Ocean had a southwestward tilt, and stretched from the western Pacific Ocean, west of the westerly ducts, to the Philippines. To the west of the PV trough, over the Pacific, some of its PV was scattered in a track around the monsoon anticyclone and over the equatorial easterly winds. Further west, over Africa, some of this PV was returning to the midlatitudes.

As for the study of McIntyre (2008) for the polar vortex, a wave-turbulence "jigsaw picture" emerges within the tropical upper troposphere. There are regions where strong PV gradients prevail and oscillatory motions dominate, and regions where Rossby waves break and their PV is mixed. The former regions are associated with the subtropical westerly jets and the latter are associated with the westerly ducts and the equatorial easterly winds. Yet, perhaps in contrast to the polar vortex, the regions where the breaking more often occurs are quite localized, and closely related to the location of the westerly ducts (Postel and Hitchman, 1999; Waugh and Polvani, 2000; Scott and Cammas, 2002; MacRitchie and Roundy, 2016).

Importantly, the variability of the tropical upper troposphere seems recurrent in the sense discussed by Cvitanović (2013) within the context of the Navier–Stokes equations. That is, while the upper tropospheric PV field never returns exactly to a previous configuration, as is expected in turbulent flows, it displays a quasi-periodic behaviour associated with Rossby wave-dynamics (Liu *et al.,* 2007; Plumb, 2007). Throughout the year, Rossby waves repeatedly propagate through the subtropical westerly jet, break within the westerly ducts, and then mix and recirculate back to midlatitudes, through the easterly winds, as eddies. The repeated breaking of Rossby waves over the westerly ducts (Waugh and Polvani, 2000) leads to advective PV fluxes towards the Tropics, and the divergent circulation over the equatorial easterly winds leads to advective PV fluxes towards the midlatitudes.

That the breaking of Rossby waves leads to PV fluxes towards the Tropics is supported by the studies of Nath *et al.* (2016; 2017), where it is hypothesized that a long-term increase in the PV and ozone concentration over the central Pacific is due to an increasing trend in the number of Rossby waves that break over the region each year. Additionally, that divergent circulations lead to advective PV fluxes towards the midlatitudes is supported by the study of Sardeshmukh and Hoskins (1988), where it is shown that a divergent circulation over the Tropics leads to Rossby wave sources that are to the north of the divergent region

and over the subtropical westerly jet. These ideas are also supported by the study of Liu *et al.* (2007), where an atmospheric model that is forced with a diabatic heating over South Asia develops a monsoon anticyclone and a continuous breaking of Rossby waves on the eastern flank of this anticyclone.

Further understanding of these advective PV fluxes can be gained by focusing on their mathematical formulation. These can be computed on an isentrope as

$$\boldsymbol{J_A} = \sigma q \boldsymbol{v}, \tag{5}$$

where $\sigma = -g^{-1}\partial P/\partial\theta$ is the isentropic mass density, $q = (\nabla \times \boldsymbol{v} + f)/\sigma$ the atmospheric PV for hydrostatic motions, $\boldsymbol{v} = (u, v, 0)$ the wind vector in isentropic coordinates, P the atmospheric pressure, and θ the potential temperature. Further, the flux through a latitude circle is given by

$$\boldsymbol{J_A} \cdot \boldsymbol{n} = \sigma q v, \tag{6}$$

where $\boldsymbol{n} = (0, -1, 0)$ is a unit vector that points towards the Equator along such a latitude circle on the isentrope.

Figures 2c and 3c show the climatological advective PV fluxes around 30°N, computed from Equation (6), for January and July. During January, negative PV fluxes (i.e. PV fluxes towards the Equator) are shifted slightly to the west of the westerly ducts, and positive PV fluxes occur elsewhere around 30°N. During July, negative PV fluxes are shifted further to the west of the westerly ducts and positive PV fluxes are again observed elsewhere around 30°N.

The legends of Figures 2c and 3c further illustrate an important property: the sum of the positive and negative advective fluxes, for both seasons, is nearly in balance. That is, along 30°N on isentrope 370 K,

$$\oint_{30°\mathrm{N}} \boldsymbol{J_A} \cdot \boldsymbol{n} dl \cong 0, \tag{7}$$

where $\boldsymbol{n}$ is a unit vector that points towards the Equator everywhere around 30°N and dl is the differential length element (e.g. Haynes and McIntyre, 1987). The balance along 30°N is more closely met during July than during January, and in both cases positive fluxes along the latitude circle are dominant. That is, along 30°N the right-hand side of Equation (7) adds up to a small positive number both during July and January.

Finally, Figures 2d and 3d show the climatological advective PV fluxes around 10°N for both January and July. The PV fluxes around 10°N have a smaller amplitude than those around 30°N, are displaced slightly further to the west relative to the 30°N fluxes, and in both cases negative fluxes along the 10°N latitude circle are dominant. As before, and in accordance with Equation (7), the positive and negative fluxes seem to be in close balance, although the balance is closer during June than during July.

We choose to study PV fluxes on the 370 K isentrope as this isentrope stays close to the tropopause, never intersects the ground and dissipative processes tend to be small on it

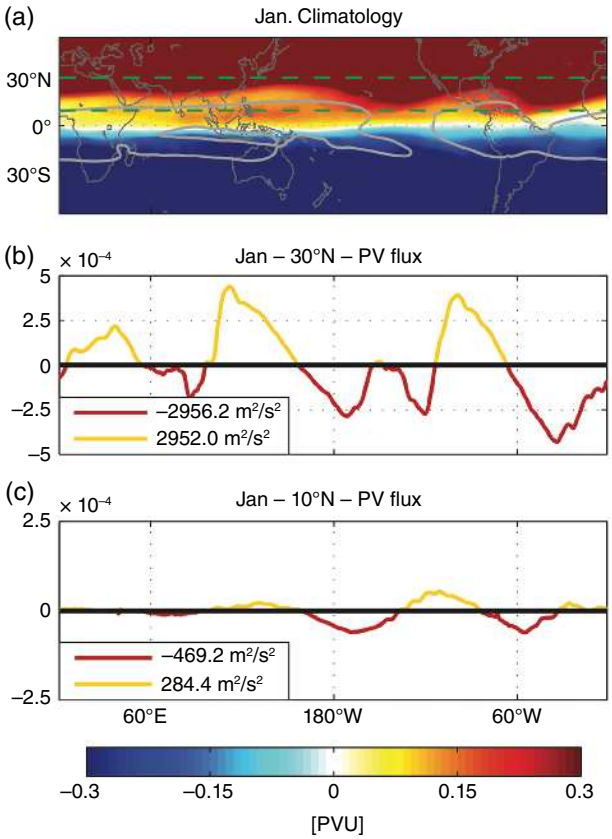

FIGURE 4 (a) Climatological 330 K PV field (PV units) for January (colour shading), boundary between westerlies and easterlies (grey contour), and lines over which PV fluxes are computed (green dashed lines). (b) PV fluxes along 30°N (red and yellow curve) and the integrated negative and positive fluxes along 30°N (legend). (c) PV fluxes along 10°N and the integrated negative and positive fluxes along 10°N. ERA-Interim data [Colour figure can be viewed at wileyonlinelibrary.com]

(e.g. Plumb, 2007). Yet, we note that PV fluxes can display a similar behaviour at lower isentropes. Figure 4, for instance, shows the climatological 330 K PV field for the month of January. As observed in the 370 K PV field, the 330 K field shows a sharp gradient associated with the subtropical westerly jet, a large-scale PV trough over the westerly ducts, and relatively low PV values to the west of this trough, extending from the west Pacific Ocean to the Indian Ocean. Interestingly, this coincides with the regions where the Madden–Julian Oscillation (MJO) often develops, intensifies and decays (Madden and Julian, 1972; Zhang and Ling, 2011).

4 | THE NATURE OF THE ISENTROPIC PV FLUXES

The near balance of PV fluxes can be understood through the so-called "impermeability theorem" of the atmosphere (Haynes and McIntyre, 1987, 1990). The theorem states two fundamental facts about PV: (a) that there are no sources or sinks of PV between isentropes that do not intersect the ground, even in the presence of diabatic and frictional processes, and (b) that a PV flux across isentropes cannot occur.

Consider the equations of PV and mass conservation for hydrostatic motions on isentropic coordinates (e.g. Holton, 2004):

$$\frac{\partial q}{\partial t} + \boldsymbol{v}\cdot\nabla_\theta q = \frac{q}{\sigma}\frac{\partial}{\partial\theta}(\sigma\dot\theta) - \frac{1}{\sigma}\boldsymbol{k}\cdot\nabla_\theta\times\left(\dot\theta\frac{\partial\boldsymbol{v}}{\partial\theta} - \boldsymbol{F}\right), \quad (8)$$

$$\frac{\partial\sigma}{\partial t} + \nabla_\theta\cdot(\sigma\boldsymbol{v}) + \frac{\partial}{\partial\theta}(\sigma\dot\theta) = 0, \quad (9)$$

where $\mathbf{F} = (F_x, F_y, 0)$ represents dissipative processes, θ is the isentropic level, $\boldsymbol{k}$ a unit vector perpendicular to the isentropic level, and $\dot\theta$ the diabatic heating term. By multiplying Equation (8) by σ and rearranging the resulting equation using Equation (9), one obtains

$$\frac{\partial(\sigma q)}{\partial t} + \nabla\cdot\boldsymbol{J} = 0, \quad (10)$$

where $\boldsymbol{J} = \boldsymbol{J_A} + \boldsymbol{J_{\dot\theta}} + \boldsymbol{J_F}$ is the total flux of PV along the isentrope, $\boldsymbol{J_{\dot\theta}} = (\dot\theta\partial v/\partial\theta, -\dot\theta\partial u/\partial\theta, 0)$ is the contribution due to diabatic heating, $\boldsymbol{J_F} = (-F_y, F_x, 0)$ is the contribution due to frictional terms, and $\boldsymbol{J_A} = \sigma q\boldsymbol{v}$ represents the advective flux of PV. Importantly, none of these fluxes has a component across isentropes, and they all point strictly along the isentropic surfaces. Furthermore, Equation (10) has no source terms, with its right-hand side always equating to zero (Haynes and McIntyre, 1987).

Equations (9) and (10) can be further simplified by considering the recursive character of the upper tropospheric levels discussed in the previous section; that is, the repeated formation of Rossby waves over the subtropical westerly jet, their breaking over the westerly ducts, and their recirculation as eddies over the equatorial easterly winds. Specifically, we can remove the temporal tendency of the equations by integrating over a long enough period (T). That is, for a given field a such that $a(x, y, t) \cong a(x, y, t+T)$, we must have

$$\int_t^{t+T}\frac{\partial a}{\partial t}dt \approx 0. \quad (11)$$

Carrying this operation for Equations (9) and (10), and assuming that advective fluxes are of first-order importance (i.e. $\boldsymbol{J_{\dot\theta}} \sim \boldsymbol{J_F} \sim 0$), we obtain the following two equations:

$$\nabla\cdot(\sigma q\boldsymbol{v}) \approx 0, \quad (12)$$

$$\nabla\cdot(\sigma\boldsymbol{v}) \approx S, \quad (13)$$

where $S = -\frac{\partial}{\partial\theta}(\sigma\dot\theta)$ is the time rate of change of the mass between isentropes; that is, a mass source between the isentropes. Note that we have not decomposed the upper tropospheric circulation into a mean term and a perturbation, so that Equations (12) and (13) apply to the full circulation features.

Equations (12) and (13) can be used to understand the close balance of PV fluxes along 30°N. Consider an atmosphere that is everywhere adiabatic except at the Equator and parallels $\pm\phi_{\text{Sink}}$ on an isentrope of the upper troposphere (a similar thought experiment to that of Charney, 1963). Assume that S, on such an isentrope, can be written as

$$S(\phi) = \frac{m}{2\pi R}\,\delta(\phi - 0) - \frac{m}{4\pi R\cos\phi_{\text{Sink}}}\,\delta(\phi + \phi_{\text{Sink}}) - \frac{m}{4\pi R\cos\phi_{\text{Sink}}}\,\delta(\phi - \phi_{\text{Sink}}), \quad (14)$$

where

$$\delta(\phi - x) = \begin{cases} 1 \to x = \phi \\ 0 \to x \neq \phi \end{cases} \quad (15)$$

is the Dirac-delta function. Equation (14) then corresponds to a zonally symmetric mass source over the Equator with two zonally symmetric sinks over parallels $\pm\phi_{\text{Sink}}$ that exactly balance the equatorial source (Figure 5; red and blue lines). That is, the global integral of S adds up to zero:

$$\iint S\,dA = 0. \quad (16)$$

Now consider a parallel ϕ_o that is between the Equator and ϕ_{Sink}. Integrating Equation (13) over the region north of ϕ_o (green dashed curve in Figure 5) shows that the mass fluxes around ϕ_o must balance the sink at ϕ_{Sink}. That is,

$$\iint\nabla\cdot(\sigma\boldsymbol{v})\,dA = \oint_{\phi_o}(\sigma\boldsymbol{v})\cdot\boldsymbol{n}\,dl = \iint S\,dA = -\frac{m}{2}. \quad (17)$$

Integrating the PV conservation equation (Equation (12)) over the same region gives

$$\iint\nabla\cdot(\sigma q\boldsymbol{v})dA = \oint_{\phi_o}(\sigma q\boldsymbol{v})\cdot\boldsymbol{n}\,dl = 2\pi R\cos\phi_o[\sigma q v]_{\phi_o} = 0, \quad (18)$$

where R is Earth's radius, and we have defined the zonal average operator for a field a, along a latitude ϕ, as

$$[a]_\phi = \frac{1}{2\pi R\cos\phi}\oint_\phi a\,dl. \quad (19)$$

Now, if we assume that $\boldsymbol{v}$ has a northward component everywhere (Figure 5a), then, in order for Equation (18) to be satisfied, σq must vanish everywhere along ϕ_o. However, if we relax this assumption, and only assume that the zonal average of $\boldsymbol{v}$ has a northward component, then Equation (18) implies that there must be a southward PV flux somewhere along ϕ_o that balances the northward flow of PV associated with the zonally averaged circulation (Figure 5b). This point was made by Haynes and McIntyre (1987, their equation 3.5) and also by Charney (1963). It also relates to the dynamics constraints pointed out by Sardeshmukh and Hoskins (1988) and Plumb (2007).

Moreover, the balance implied in Equation (18) is also consistent with the studies of Lee (1999) and Dima *et al.* (2005), where they studied the mean zonally averaged circulation of the Tropics, and observed a close balance between the momentum transport by the meridional circulation and the momentum transport by the zonal eddies.[3] In fact,

[3]Note that by "zonal eddies" we mean stationary waves in the tropical upper troposphere; as opposed to "eddies", by which we mean PV anomalies that result from the breaking of Rossby waves.

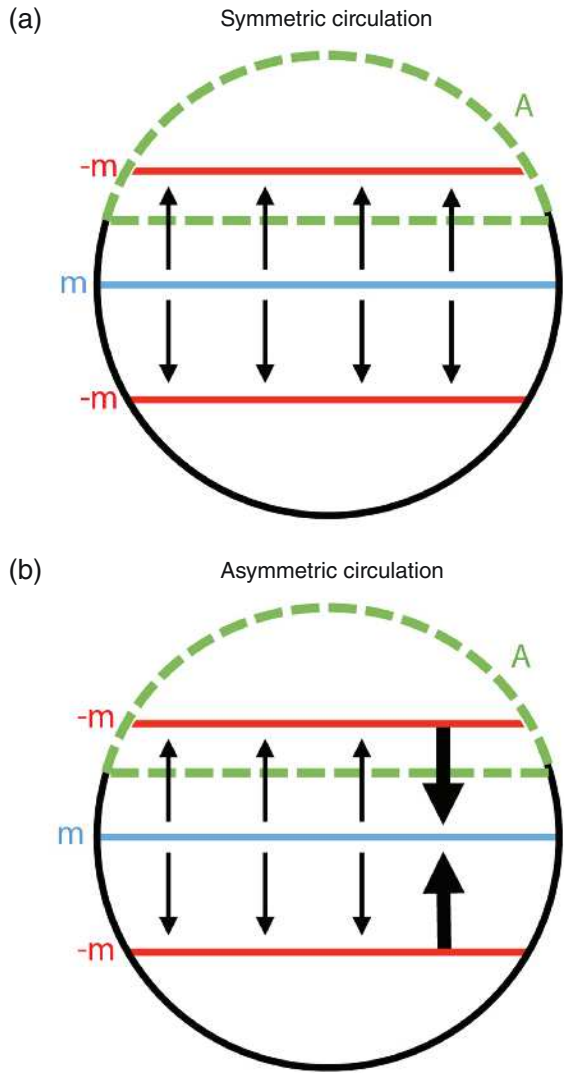

FIGURE 5 Idealized flow in an upper tropospheric isentrope that surrounds the globe. Blue lines represent mass sources and red lines represent mass sinks. A circulation is expected to develop, going from the mass sources towards the mass sinks. We consider two possibilities: (a) a circulation that goes everywhere poleward, and (b) a circulation that goes poleward in a zonally averaged sense. In the absence of dissipation and diabatic processes, a circulation that goes everywhere poleward can only develop if the PV field is zero everywhere along the poleward flow (black arrows, (a)), so that the PV flux through a given latitude (green dashed curve) is exactly zero. A circulation that goes poleward in a zonally averaged sense can develop even if its PV field is not zero everywhere. In this case equatorward return fluxes of PV (big black arrows, (b)) must develop in response to the poleward PV fluxes; moreover, the fluxes should balance each other [Colour figure can be viewed at wileyonlinelibrary.com]

Equation (18) implies such momentum balance. This can be easily shown by separating the flow into its zonal average and zonal eddy components, and assuming that the horizontal divergence is dominant in the continuity equation. This leads, using Cartesian coordinates for simplicity, to the following equation:

$$[\sigma q v] \cong (f + [\xi])[v] - \frac{\partial [v^* u^*]}{\partial y} = 0, \qquad (20)$$

where $\xi = \nabla \times \boldsymbol{v}$ is the relative vorticity of the atmosphere and the asterisks denote deviations from the zonal average (the zonal eddies). The first term on the right-hand side is the momentum transport by the zonally averaged meridional circulation, and the second term is the momentum transport by the zonally averaged zonal eddies.

Thus, Equation (20) shows that both the momentum transport by the zonally averaged meridional circulation and the momentum transport by the zonally averaged zonal eddies are determined by the global balance of PV. This explains the observation of Dima *et al.* (2005) that a stronger meridional circulation is accompanied by stronger zonal eddies in the tropical upper troposphere. Such an observation can be understood on the basis that, in order to conserve PV, the PV that enters the Tropics is balanced, to first order, by the PV that leaves it. Importantly, it should also be noted that to arrive at Equation (20) the recursive character of the circulation had to be assumed (Equation (11)); that is, the repeated formation, propagation and breaking of Rossby waves are necessary in order for Equation (20) to hold approximately true.

4.1 | The effect of the PV fluxes in the upper tropospheric circulation

Equation (18) represents the first-order balance of the PV budget,[4] but it is only a first-order approximation as the advective PV fluxes ($\boldsymbol{J_A}$) are never exactly in balance, and both $\boldsymbol{J_\theta}$ and $\boldsymbol{J_F}$ will usually have finite values. Importantly, imbalances of the advective PV fluxes, that is, the existence of finite frictional and diabatic terms, are required to maintain the features of the tropical upper tropospheric circulation discussed in the introduction.

To see this, consider the equations of motion for a hydrostatic atmosphere written as in Hsu and Arakawa (1990), which emphasize the role of PV fluxes:

$$\frac{\partial \boldsymbol{v}}{\partial t} = -\sigma q \boldsymbol{k} \times \boldsymbol{v} - \nabla_\theta (M + K_E) - \dot{\theta} \frac{\partial \boldsymbol{v}}{\partial \theta} + \boldsymbol{F}, \qquad (21)$$

where $K_E = \frac{1}{2}\boldsymbol{v}^2$ is the kinetic energy, $M = c_p T + \Phi$ is the Montgomery stream function, T the temperature, Φ the geopotential, and c_p the specific heat constant at constant pressure. The zonal component of Equation (21) is simply

$$\frac{\partial u}{\partial t} = \sigma q v - \frac{\partial}{\partial x}(M + K_E) - \dot{\theta} \frac{\partial u}{\partial \theta} + F_x. \qquad (22)$$

Taking the zonal average of Equation (22), dropping the temporal derivatives by assuming either a steady state or a recurrent state (Equation (11)), and assuming that $F_x = -ku$, where k is a linear damping coefficient, we obtain a relation between the zonally averaged features of the circulation, the zonally averaged PV fluxes, and the momentum fluxes due to diabatic processes. This relation reads

$$[u] \approx \frac{1}{k} \left\{ [\sigma q v] - \left[\dot{\theta} \frac{\partial u}{\partial \theta} \right] \right\}. \qquad (23)$$

[4] Which as we saw (Equation (20)) and according to previous literature (e.g. Lee, 1999; Dima *et al.*, 2005), is also the first-order balance in the momentum equation.

Moreover, in an adiabatic atmosphere,

$$[u] \approx \frac{1}{k}\,[\sigma q v]. \tag{24}$$

Thus, the imbalance of the advective PV fluxes can have a direct effect on the zonally averaged meridional winds. Of course, it should be kept in mind that using linear damping is not ideal, as it might not correctly represent how PV is dissipated, and that diabatic terms are important for the tropical circulation, making Equation (24) an inaccurate approximation. However, it is important to note here that Equation (23) points to the dissipation of PV as a process that supports the maintenance of the zonal winds in the tropical upper troposphere.

To summarize, we have shown in this section that an upper tropospheric mass flux imposed by a mean meridional circulation (Equation (17)) leads to PV fluxes, in and out from the tropical upper troposphere, that closely balance each other as a result of the global conservation of PV (Equation (18)). We have hypothesized that such a balance is possible due to the recurrent character of the tropical upper tropospheric circulation (Equation (11)). And that the dissipation of PV over the Tropics, associated to these PV fluxes in and out of the Tropics, helps to maintain the upper tropospheric circulation (Equation (23)).

5 | A SHALLOW-WATER MODEL OF THE UPPER TROPOSPHERE

Following Hsu and Plumb (2000), we can explore the ideas discussed above with experiments that use the shallow-water model introduced in section 2. The shallow-water model is a highly idealized model of the upper troposphere and has no representation of the vertical momentum transport of the atmosphere (i.e. $\dot{\theta}\partial u/\partial\theta$ is absent). Yet, its use is a good approach here for at least three reasons. First, the atmospheric equations of motion along isentropes are similar to the equations of motion of the shallow-water model (e.g. Vallis, 2017). Second, we can choose the dissipative terms of the model to be a linear damping, so that an analogous equation to Equation (24) applies. Third, the concept of recurrence can be easily exploited as the results of the model turn out to be periodic (Hsu and Plumb, 2000; Plumb, 2007).

The curl of the shallow-water momentum equation (Equation (1)) yields an equation analogous to Equation (10):

$$\frac{\partial hq}{\partial t} + \nabla\cdot(\boldsymbol{u}hq + \boldsymbol{J_F}) = 0, \tag{25}$$

where $\boldsymbol{J_F} = (-F_y, F_x, 0)$, $\boldsymbol{F} = (F_x, F_y) = -k\boldsymbol{u}$, and k is the linear damping coefficient. As for Equation (10), there are no sources of PV in the shallow-water layer even when frictional forces and mass sources are present. This last statement is analogous to the impermeability theorem of the atmosphere.[5]

Now, if advective PV fluxes are dominant, then

$$\frac{\partial hq}{\partial t} + \nabla\cdot(\boldsymbol{u}hq) \cong 0. \tag{26}$$

Further, as the shallow-water model results are periodic, that is, as $a(x,y,t) = a(x,y,t+T)$ for a given field a and a period T, then

$$\int_t^{t+T} \frac{\partial a}{\partial t}dt = 0, \tag{27}$$

which is an exact version of Equation (11). The PV flux and mass conservation equations (Equations (26) and (2)) then simplify to

$$\nabla\cdot(\boldsymbol{u}hq) \cong 0, \tag{28}$$

$$\nabla\cdot(h\boldsymbol{v}) = S, \tag{29}$$

where S is given by Equation (3). By analogous arguments to those of Equation (12) through to Equation (18), these last two equations imply that, when advective terms are dominant, there cannot be a circulation that goes everywhere poleward in the shallow-water model and that alternating positive and negative PV fluxes along latitude circles will develop instead.

Moreover, the effect of PV fluxes on the shallow-water model is analogous to that between isentropes of an adiabatic atmosphere (Equation (24)). To see this, consider the zonal component of Equation (1):

$$\frac{\partial u}{\partial t} - qhv = -\frac{\partial}{\partial x}(K_E + gh) - ku. \tag{30}$$

Integrating over a period (Equation (27)), or in steady state, we obtain

$$-qhv = -\frac{\partial}{\partial x}(K_E + gh) - ku, \tag{31}$$

and taking the zonal average gives

$$[u] = \frac{1}{k}[qhv]. \tag{32}$$

Equation (32) is exact when the results from the shallow-water model are either periodic or steady. Thus, in such cases, there is a clear relation between the PV fluxes and the circulation features of the shallow-water model.

5.1 | Results for two modelling experiments

We present results of two experiments conducted with the shallow-water model. The first experiment, which we refer to as the *maritime experiment*, is intended to represent the effect that deep convection over the maritime continent has on the tropical upper troposphere, so as to represent the observed circulation during January. The second experiment, which

[5]This can be easily appreciated if one derives Equation (25) by following an analogous procedure to that used in deriving Equation (10); that is, by multiplying the corresponding shallow-water PV equation by h and using Equation (2) to obtain Equation (25). However, the procedure followed in the main text has the advantage of showing that Equation (25) is just a version of the absolute vorticity equation that emphasizes PV fluxes.

we refer to as the *monsoon experiment*, is intended to represent the effect that deep convection over South Asia and the sensible heating of the Tibetan Plateau have on the upper tropospheric circulation, so as to represent the observed circulation during July. These experiments allow us to explore the ideas put forward at the end of section 4.

For the maritime continent experiment, we force the shallow-water model using an equilibrium height (h_e, Equation (3)) that peaks over the Equator. Specifically, we set $H = 500$ m, $\lambda_o = 0$, $\phi_o = 0$, $A = 30{,}000$ m, $\sigma_\phi = 6°$, $\sigma_\lambda = 10°$, and $\tau = \frac{1}{10}\text{day}^{-1}$ in Equations (3) and (4). We include the mass forcing S from the first time step, and leave it on for the rest of the experiment. A steady state is reached after the initial transients of the model dissipate.

For the monsoon experiment we force the shallow-water model using an equilibrium height (h_e) that peaks over 30°N. We set $H = 500$ m, $\lambda_o = 0$, $\phi_o = 30°$, $A = 30{,}000$ m, $\sigma_\phi = 6°$, $\sigma_\lambda = 10°$, and $\tau = \frac{1}{10}\text{day}^{-1}$. As before, we include the mass forcing S from the first time step, and leave it on for the rest of the experiment. A periodic, or closely periodic, solution is reached after the initial transients dissipate.

Figure 6 shows different stages of the monsoon experiment. While the experiment turns out to be periodic, it also displays characteristics that are often associated with geophysical turbulence. The PV field is constantly pulled from midlatitudes towards the Tropics, forming a PV trough to the east of the forcing. This trough becomes thinner with time, folds onto itself, and then detaches from the main trough as an eddy. The whole process is then one that facilitates the mixing of PV over the equatorial region, allowing dissipative terms to act more efficiently.

The steady-state PV fields for the maritime continent experiment and the time-averaged PV fields for the monsoon experiment are shown in Figures 7a and 8a, respectively. As found in the observed upper tropospheric circulation (Figures 2 and 3), both experiments develop subtropical westerly jets that are associated with sharp PV gradients over the midlatitudes, westerly ducts that are associated with midlatitude PV troughs that extend towards the Equator, and equatorial easterly winds that are to the west of these midlatitude PV troughs. However, there are also important differences between the experimental and the observational fields. Results from the maritime continent experiment show equatorial easterly winds extending over a much smaller region than in the real atmosphere and, accordingly, the westerly ducts extend over a much larger region. For the monsoon experiment, the equatorial easterly winds completely surround the Equator and have a much more zonal structure than in the real atmosphere. Westerly ducts are also present in this experiment, but appear as small intrusions of westerly winds into the equatorial easterlies. Yet, as found in the observed fields, to the south of these westerly ducts the speed of the equatorial easterly winds decreases considerably.

Figures 7b and 8b show the advective PV fluxes computed along 30°N for the shallow-water experiments. The same

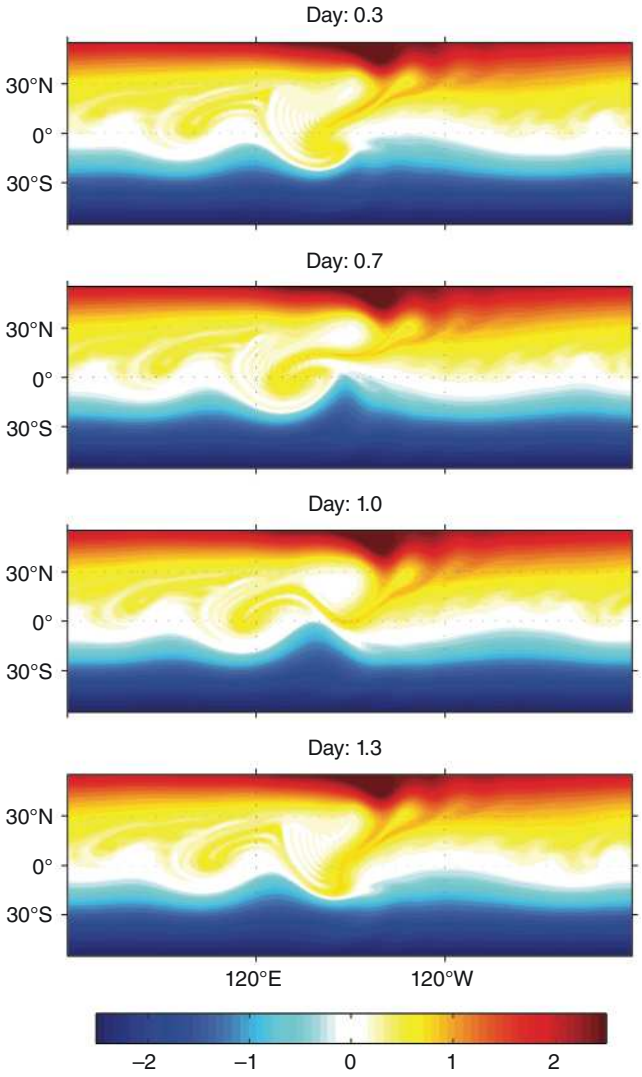

FIGURE 6 Periodic solution of the shallow-water monsoon experiment at four different times during the integration. The potential vorticity field is shown (colour shading, units are 10^{-7} $\text{m}^{-1}\text{s}^{-1}$). Notice how the PV field is stretched, folded, and mixed [Colour figure can be viewed at wileyonlinelibrary.com]

fields but along 10°N are shown in Figures 7c and 8c. As found in the observed upper troposphere, PV fluxes towards the Equator around latitude circles are shifted slightly to the west of the westerly ducts, and poleward PV fluxes occur elsewhere around these latitude circles.

Examining the legends of Figures 7b,c and 8b,c shows that the balance implied by Equation (28) was more closely met in the monsoon experiment near 30°N, where the zonally average winds were near zero (as is expected from Equation (32)), than near 30°N in the maritime experiment. Around 10°N of the monsoon experiment and the maritime continent experiment, there was a strong imbalance between the northward and southward PV fluxes; consistent with the winds that developed around these latitudes, but unlike what is seen in observations. The strong imbalance of the monsoon experiment around 10°N was most likely due to the "turbulent" nature of the simulation and to the high values used for the linear dissipation coefficient, which allowed

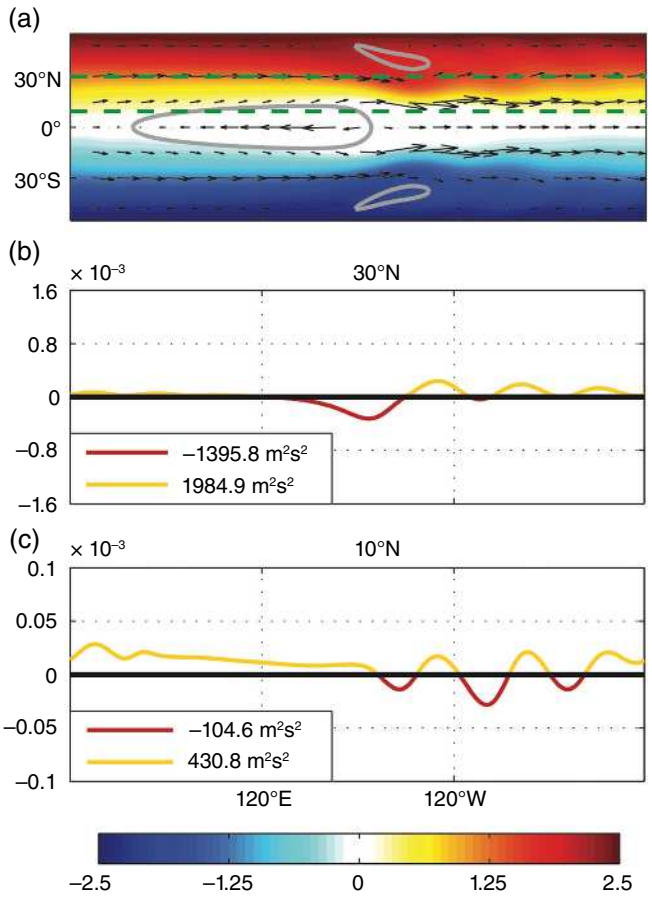

FIGURE 7 (a) Steady-state PV field of the shallow-water maritime continent experiment (colour shading, units are 10^{-7} $m^{-1}s^{-1}$) and its steady state winds (black arrows). (b) PV fluxes along 30°N (red and yellow curve) and the integrated negative and positive fluxes along 30°N (legend). (c) PV fluxes along 10°N and the integrated negative and positive fluxes along 10°N [Colour figure can be viewed at wileyonlinelibrary.com]

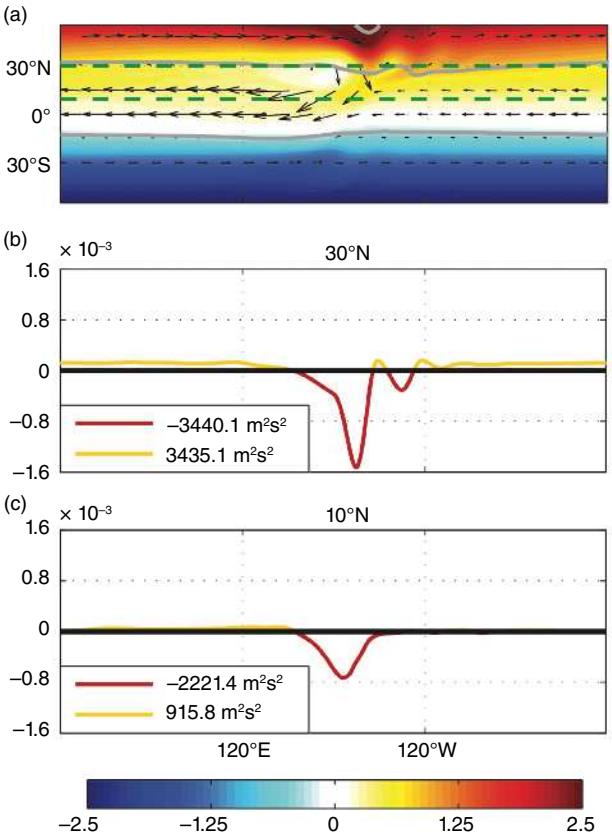

FIGURE 8 (a) Time-averaged PV field of the shallow-water monsoon experiment (colour shading, units are 10^{-7} $m^{-1}s^{-1}$) and its time-averaged winds (black arrows). (b) Time-averaged PV fluxes along 30°N (red and yellow curve) and the integrated negative and positive fluxes along 30°N (legend). (c) Time-averaged PV fluxes along 10°N and the integrated negative and positive fluxes along 10°N [Colour figure can be viewed at wileyonlinelibrary.com]

dissipative processes to act efficiently. The strong imbalance of the maritime continent experiments was also likely due to dissipative processes.

Finally, Figure 9 shows the right and left sides of Equation (32) for both experiments as a function of latitude. The red dashed curves correspond to the steady, or temporally averaged, zonal average of the meridional PV fluxes divided by the dissipation coefficient (i.e.$[hqv]/k$). The black curves correspond to the steady, or temporally averaged, zonally averaged zonal winds (i.e.$[u]$). In both experiments, in accord with Equation (32), both curves closely follow each other. The equatorial easterly winds are associated with negative zonal averages of the PV fluxes, and the subtropical westerly jet is associated with positive zonal averages of the PV fluxes. For the monsoons experiment, where the periodic solution is obtained, Figure 9b also shows that there is a large variation of the zonal average of transient PV fluxes (light-blue curves), whose temporal average results in the zonally averaged winds. This shows that the imbalance of PV fluxes in the shallow-water model maintains the mean zonally averaged circulation, and suggests a similar role for PV fluxes in the real atmosphere.

6 | DISCUSSION

The simplified forms of the absolute vorticity and mass continuity equations (Equations (12) and (13)) point to a balance in the tropical upper troposphere. The balance is both for mass fluxes and for advective PV fluxes. This balance has been previously studied by several authors (e.g. Haynes and McIntyre, 1987), and this article stresses its relevance for the tropical upper troposphere.

The dynamics of the tropical upper troposphere suggests that the balance is achieved via Rossby-wave dynamics. To illustrate this balance, consider a hypothetical atmosphere subject to persistent deep tropical convection over, say, the maritime continent. Such persistent convection would be associated with divergent circulations in the tropical upper troposphere, which would constantly push the subtropical westerly jet towards the Poles by advecting PV poleward and would, therefore, set up an advective PV flux towards the Poles. In turn, this poleward advection would constantly trigger Rossby waves on the subtropical westerly jets (as in Sardeshmukh and Hoskins, 1988), and these waves would progress along the jet until reaching the westerly ducts. Once over the ducts, these Rossby waves could break and, as a

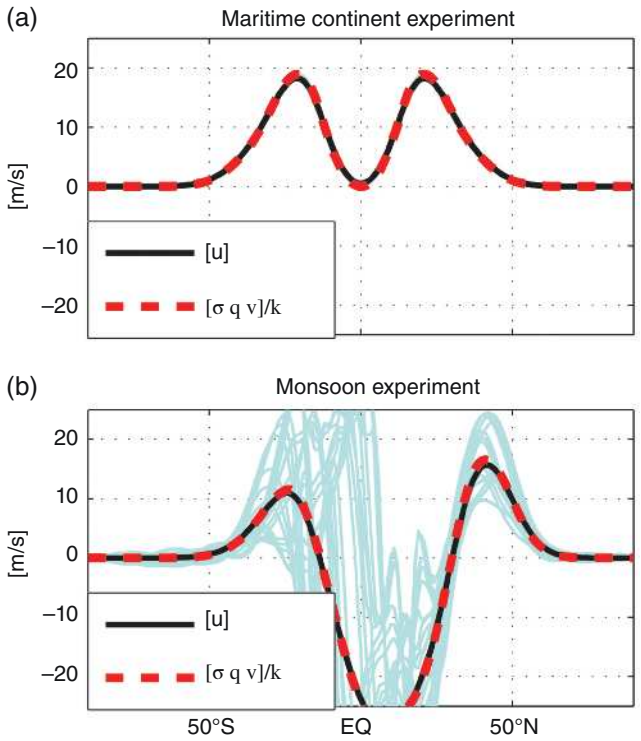

FIGURE 9 (a) Steady-state zonally averaged zonal winds (black curve) and the zonally averaged PV fluxes for the maritime continent experiments (red dashed curve). (b) Temporally and zonally averaged zonal winds (black curve), temporally and zonally averaged PV fluxes (red dashed curve), and the instantaneous zonally averaged PV fluxes for different time steps of the simulation (light-cyan curves). The PV fluxes were divided by the dissipation coefficient in both panels [Colour figure can be viewed at wileyonlinelibrary.com]

result of the breaking, PV would be advected back towards the Tropics; which would set up an advective PV flux towards the Equator. This study suggests that the equatorward PV flux due to the breaking Rossby waves[6] closely balances the poleward PV flux associated with the persistent deep convection that triggered the waves in the first place. As is evident in Figures 2 and 3, a close balance between poleward and equatorward fluxes is indeed observed in ERA-Interim data, and that this balance is at least in part achieved via Rossby-wave dynamics can be seen, for instance, in the supplementary movie of Ortega *et al.* (2017).

The importance of Rossby wave-breaking is also in line with the studies of Moore *et al*. (2010) and MacRitchie and Roundy (2016), which show that the MJO modulates anticyclonic wave breakings (i.e. Rossby wave breakings) over the central Pacific Ocean. Moreover, MacRitchie and Roundy suggest that this breaking is also associated with convergent circulations over the Pacific Ocean, an idea that is consistent with velocity potential composites of the MJO, as these tend to show alternating divergent and convergent signals over the Tropics (Ventrice *et al.,* 2013). Our study suggests a mechanism to help explain these results in a simple framework (Equations (11)–(13)), pointing at the conservation of global PV as an important dynamical constraint for the large-scale tropical circulation.[7]

A coupling of the subtropical westerly jet, the westerly ducts and TUTTs, and the equatorial easterly winds is suggested by the longitudinal location of the poleward and equatorward advective PV fluxes, shown in Figures 2 and 3, and by the imbalances in these fluxes (Equation (23)). Equivalently, this can also be seen as suggesting a coupling of Hadley and Walker cells. That is, as pointed out by Nath *et al.* (2016), and expected from the study of Sardeshmukh and Hoskins (1988), convection over the maritime continent not only influences the Hadley cell (as in Held and Hou, 1980; Lindzen and Hou, 1988; Plumb and Hou, 1992) but also triggers Rossby waves (see also Plumb, 2007) that influences the Walker circulation.

Finally, that the imbalance of the advective PV fluxes affects the mean winds of the tropical upper troposphere (Equation (23)) is expected in light of theories of the mean meridional circulation and theories of eddy-mean flow interactions. As shown by Lee (1999) and Dima *et al.* (2005), the mean meridional circulation decelerates the zonally averaged tropical winds while the eddy terms accelerate these. These two effects are intimately linked through the conservation of global PV and can affect the mean winds as shown by Equations (20) and (23). The recurrent character of the tropical upper troposphere (Equation (11)) is what seems to allow for such balance. Thus, the repeated formation, propagation and breaking of Rossby waves are important for the maintenance of the circulation of the tropical upper troposphere. Moreover, the periodicity of the shallow-water monsoon experiment allowed us to explore this last point, as we could exactly link the effect of imbalances of the PV fluxes with the mean zonal winds of the experiment, as made clear in Equation (32) and Figure 9.

Importantly, the periodicity of the shallow-water monsoon experiment also points to recent advances in chaos theories, where the periodic solutions of the dynamical systems, even if unstable, are shown to be crucial to understanding these systems (Christiansen *et al.,* 1997; Cvitanović *et al.,* 2012; Cvitanović, 2013).[8] Thus, these chaos theories could provide a basis for studying the dynamics of the tropical upper troposphere, which can be thought of as a chaotic, but recurrent, dynamical system. It seems reasonable to expect that further research aiming at applying these chaos theories to geophysical

[6]Note that the role of Rossby-wave dynamics in maintaining such a balance seems analogous to that of Lighthill radiation in the context of maintaining geostrophic balance (McIntyre, 2001), where gravity waves are constantly radiated to achieve geostrophic balance. Here, however, Rossby waves are the entities being constantly radiated, and the *balance* might not be a steady but a recurring and turbulent state of the upper troposphere.

[7]For smaller-scale circulations, other effects are also important. For instance, Waugh and Funatsu (2003) linked the breaking of Rossby waves over the central Pacific with tropical convection that was triggered by isentropic lifting.

[8]For a quick introduction to these ideas, go to http://www.cns.gatech.edu/~gibson/research/tutorial/.

problems would lead to a better understanding of fundamental matters such as eddy–mean flow interactions.

ACKNOWLEDGEMENTS

We thank Annalisa Bracco, Predrag Cvitanović, Fabrizio Falasca and Michael McIntyre for useful discussion during the course of this research project. We extend our gratitude to the two anonymous reviewers of the original manuscript for their insightful comments. Funding support for this research project was provided by the Climate Dynamics Division of the National Science Foundation under grants NSF-AGS 0965610 and NSF-AGS 1638256. This research was conducted in the School of Earth and Atmospheric Sciences at the Georgia Institute of Technology.

REFERENCES

Arakawa, A. and Lamb, V.R. (1981) A potential enstrophy and energy conserving scheme for the shallow water equations. *Monthly Weather Review*, 109, 18–36.

Chang, E.K. and Yu, D.B. (1999) Characteristics of wave packets in the upper troposphere. Part I: Northern Hemisphere winter. *Journal of the Atmospheric Sciences*, 56, 1708–1728.

Charney, J.G. (1963) A note on large-scale motions in the Tropics. *Journal of the Atmospheric Sciences*, 20(6), 607–609.

Christiansen, F., Cvitanovic, P. and Putkaradze, V. (1997) Spatiotemporal chaos in terms of unstable recurrent patterns. *Nonlinearity*, 10, 55.

Cvitanović, P. (2013) Recurrent flows: the clockwork behind turbulence. *Journal of Fluid Mechanics*, 726, 1–4.

Cvitanović, P., Artuso, R., Mainieri, R., Tanner, G. and Vattay, G. (2012) *Chaos: Classical and Quantum*. Copenhagen: Niels Bohr Institute.

Dee, D.P., Uppala, S.M., Simmons, A.J., Berrisford, P., Poli, P., Kobayashi, S., Andrae, U., Balmaseda, M.A., Balsamo, G., Bauer, P. and Bechtold, P. (2011) The ERA-Interim reanalysis: configuration and performance of the data assimilation system. *Quarterly Journal of the Royal Meteorological Society*, 137(656), 553–597.

Dima, I.M., Wallace, J.M. and Kraucunas, I. (2005) Tropical zonal momentum balance in the NCEP reanalyses. *Journal of the Atmospheric Sciences*, 62(7), 2499–2513.

Garny, H. and Randel, W.J. (2013) Dynamic variability of the Asian monsoon anticyclone observed in potential vorticity and correlations with tracer distributions. *Journal of Geophysical Research: Atmospheres*, 118(24), 13421–13433.

Gill, A.E. (1980) Some simple solutions for heat-induced tropical circulation. *Quarterly Journal of the Royal Meteorological Society*, 106(449), 447–462.

Gray, W.M. (1968) Global view of the origin of tropical disturbances and storms. *Monthly Weather Review*, 96, 669.

Hack, J.J. and Jakob, R. (1992) *Description of a global shallow water model based on the spectral transform method*. National Center for Atmospheric Research. NCAR/TN-343+STR.

Haynes, P.H. and McIntyre, M.E. (1987) On the evolution of vorticity and potential vorticity in the presence of diabatic heating and frictional or other forces. *Journal of the Atmospheric Sciences*, 44, 828–841.

Haynes, P.H. and McIntyre, M.E. (1990) On the conservation and impermeability theorems for potential vorticity. *Journal of the Atmospheric Sciences*, 47, 2021–2031.

Held, I.M. and Hou, A.Y. (1980) Nonlinear axially symmetric circulations in a nearly inviscid atmosphere. *Journal of the Atmospheric Sciences*, 37(3), 515–533.

Hoerling, M.P. (1992) Diabatic sources of potential vorticity in the general circulation. *Journal of the Atmospheric Sciences*, 49(23), 2282–2292.

Holton, J.R. (2004) *An introduction to dynamic meteorology*. Burlington, MA: Academic Press.

Hoskins, B.J. (2014) Cross-equatorial flow and the Hadley Cell. *American Geophysical Union 2014 Fall meeting*, Bjerknes Lecture. Available at: https://www.youtube.com/watch?v=XZLdT1qUQDE.

Hsu, C.J. and Plumb, R.A. (2000) Nonaxisymmetric thermally driven circulations and upper-tropospheric monsoon dynamics. *Journal of the Atmospheric Sciences*, 57, 1255–1276.

Hsu, Y.-J.G. and Arakawa, A. (1990) Numerical modeling of the atmosphere with an isentropic vertical coordinate. *Monthly Weather Review*, 118, 1933–1959.

Kiladis, G.N. and Weickmann, K.M. (1992) Extratropical forcing of tropical Pacific convection during northern winter. *Monthly Weather Review*, 120, 1924–1939.

Knippertz, P. (2007) Tropical–extratropical interactions related to upper-level troughs at low latitudes. *Dynamics of Atmospheres and Oceans*, 43, 36–62.

Koteswaram, P. (1958) The easterly jet stream in the Tropics. *Tellus*, 10, 43–57.

Koteswaram, P. and George, C.A. (1958) On the formation of monsoon depression on the Bay of Bengal. *Indian Journal of Meteorology & Geophysics*, 9, 9–22.

Lee, S. (1999) Why are the climatological zonal winds easterly in the equatorial upper troposphere? *Journal of the Atmospheric Sciences*, 56(10), 1353–1363.

Lindzen, R.S. and Hou, A.V. (1988) Hadley circulations for zonally averaged heating centered off the Equator. *Journal of the Atmospheric Sciences*, 45(17), 2416–2427.

Liu, Y., Hoskins, B.J. and Blackburn, M. (2007) Impact of Tibetan orography and heating on the summer flow over Asia. *Journal of the Meteorological Society of Japan. Series II*, 85, 1–19.

MacRitchie, K. and Roundy, P.E. (2016) The two-way relationship between the Madden–Julian oscillation and anticyclonic wave breaking. *Quarterly Journal of the Royal Meteorological Society*, 142(698), 2159–2167.

Madden, R.A. and Julian, P.R. (1972) Description of global-scale circulation cells in the Tropics with a 40–50 day period. *Journal of the Atmospheric Sciences*, 29, 1109–1123.

McIntyre, M.E. (2001) Balance, potential-vorticity inversion, Lighthill radiation, and the slow quasi-manifold. In: *IUTAM Symposium on Advances in Mathematical Modelling of Atmosphere and Ocean Dynamics*, 2–7 July 2000, Limerick, Ireland. Dordrecht: Springer, pp. 45–68.

McIntyre, M.E. (2008) Potential-vorticity inversion and the wave-turbulence jigsaw: Some recent clarifications. *Advances in Geosciences*, 15, 47–56.

McIntyre, M.E. and Palmer, T.N. (1983) Breaking planetary waves in the stratosphere. *Nature*, 305, 593–600.

Moore, R.W., Martius, O. and Spengler, T. (2010) The modulation of the subtropical and extratropical atmosphere in the Pacific basin in response to the Madden–Julian oscillation. *Monthly Weather Review*, 138(7), 2761–2779.

Nath, D., Chen, W., Graf, H.F., Lan, X., Gong, H., Nath, R., Hu, K. and Wang, L. (2016) Subtropical potential vorticity intrusion drives increasing tropospheric ozone over the tropical central Pacific. *Scientific Reports*, 6, 21370.

Nath, D., Chen, W. and Lan, X. (2017) Long-term trend in potential vorticity intrusion events over the Pacific Ocean: role of global mean temperature rise. *Journal of Meteorological Research*, 31, 906–915.

Ortega, S., Webster, P.J., Toma, V. and Chang, H.R. (2017) Quasi-biweekly oscillations of the South Asian monsoon and its co-evolution in the upper and lower troposphere. *Climate Dynamics*, 49, 3159–3174.

Plumb, R.A. (2007) Dynamical constraints on monsoon circulations. In: Schneider, T. and Sobel, A. (Eds.) *The Global Circulation of the Atmosphere*. Princeton, NJ: Princeton University Press. ISBN 9780691121819.

Plumb, R.A. and Hou, A.Y. (1992) The response of a zonally symmetric atmosphere to subtropical thermal forcing: Threshold behavior. *Journal of the Atmospheric Sciences*, 49(19), 1790–1799.

Postel, G.A. and Hitchman, M.H. (1999) A climatology of Rossby wave breaking along the subtropical tropopause. *Journal of the Atmospheric Sciences*, 56, 359–373.

Sadler, J.C. (1976) A role of the tropical upper tropospheric trough in early season typhoon development. *Monthly Weather Review*, 104(10), 1266–1278.

Sardeshmukh, P.D. and Hoskins, B.J. (1988) The generation of global rotational flow by steady idealized tropical divergence. *Journal of the Atmospheric Sciences*, 45(7), 1228–1251.

Scott, R.K. and Cammas, J.P. (2002) Wave breaking and mixing at the subtropical tropopause. *Journal of the Atmospheric Sciences*, 59, 2347–2361.

Scott, R.K., Cammas, J.P., Mascart, P. and Stolle, C. (2001) Stratospheric filamentation into the upper tropical troposphere. *Journal of Geophysical Research*, 106(D11), 11835–11848.

Slingo, J.M. (1998) Extratropical forcing of tropical convection in a northern winter simulation with the UGAMP GCM. *Quarterly Journal of the Royal Meteorological Society*, 124, 27–51.

Tomas, R.A. and Webster, P.J. (1994) Horizontal and vertical structure of cross-equatorial wave propagation. *Journal of the Atmospheric Sciences*, 51, 1417–1430.

Vallis, G.K. (2017) *Atmospheric and Oceanic Fluid Dynamics*. Cambridge: Cambridge University Press.

Ventrice, M.J., Wheeler, M.C., Hendon, H.H., Schreck, C.J., III, Thorncroft, C.D. and Kiladis, G.N. (2013) A modified multivariate Madden–Julian oscillation index using velocity potential. *Monthly Weather Review*, 141(12), 4197–4210.

Waugh, D.W. and Funatsu, B.M. (2003) Intrusions into the tropical upper troposphere: three-dimensional structure and accompanying ozone and OLR distributions. *Journal of the Atmospheric Sciences*, 60(4), 637–653.

Waugh, D.W. and Polvani, L.M. (2000) Climatology of intrusions into the tropical upper troposphere. *Geophysical Research Letters*, 27, 3857–3860.

Webster, P.J. (1972) Response of the tropical atmosphere to local, steady forcing. *Monthly Weather Review*, 100(7), 518–541.

Webster, P.J. and Chang, H.R. (1988) Equatorial energy accumulation and emanation regions: impacts of a zonally varying basic state. *Journal of the Atmospheric Sciences*, 45(5), 803–829.

Webster, P.J. and Holton, J.R. (1982) Cross-equatorial response to middle-latitude forcing in a zonally varying basic state. *Journal of the Atmospheric Sciences*, 39, 722–733.

Wu, G., Duan, A., Liu, Y., Mao, J., Ren, R., Bao, Q., He, B., Liu, B. and Hu, W. (2014) Tibetan Plateau climate dynamics: recent research progress and outlook. *National Science Review*, 2(1), 100–116.

Zhang, C. and Ling, J. (2011) Potential vorticity of the Madden–Julian Oscillation. *Journal of the Atmospheric Sciences*, 69, 65–78.

How to cite this article: Ortega S, Webster PJ, Toma V, Chang H-R. The effect of potential vorticity fluxes on the circulation of the tropical upper troposphere. *Q J R Meteorol Soc* 2018;144:848–860. https://doi.org/10.1002/qj.3261